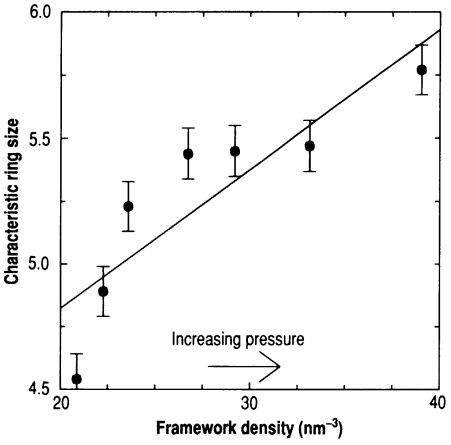

Fig. 3. The characteristic ring size, K^* (Eq. 2), calculated from the simulated structures of SiO_2 liquid at 2000 K as a function of framework density. The points represent averages of the two simulations at each pressure (*10*). The error bars indicate the uncertainty, estimated by the average difference between the simulations. Deviations from the linear trend in excess of the error bars are likely because of the simplifying assumptions built into the theory: the standard deviation from the best fit line (0.072) is similar to that observed in the much larger sample of crystalline tectosilicates (0.054) (*6*).

lar increase in K^* with increasing framework density in crystalline tectosilicates (*6*). We attribute these results to the greater pruning efficiency of small rings and their consequent tendency to form sparse, low-density frameworks. Thus, our theory illustrates the close relation between ring statistics and the density of framework structures and rationalizes compression in the liquid.

Our simulations illustrate the remarkable degree of topological variation possible in a tetrahedrally bonded liquid. Pressure-induced changes in the liquid's topology are systematic and are mimicked by crystalline framework structures (*6*)—both show a tendency for characteristic ring size to increase with increasing density. These results do not support the intuitive association of small rings with high density and lead us to conclude that the liquid compresses primarily by increasing the size of its rings. The topological compression mechanism, which is unavailable to crystals, may also facilitate efficient compression of natural magmas and liquid-crystal density inversion in Earth's upper mantle.

REFERENCES AND NOTES

1. J. Canton, *Trans. R. Soc.* (1762), p. 640; *ibid* (1764), p. 261. See P. W. Bridgman, *The Physics of High Pressure* (Macmillan, New York, 1931), for a historical overview.
2. P. W. Bridgman, *Z. Kristallogr.* 67, 363 (1928); L. Pauling, *ibid.* 69, 35 (1928).
3. L. Stixrude and M. S. T. Bukowinski, *Phys. Chem. Miner* 16, 199 (1988).
4. ———, *Geophys Res Lett.* 16, 1403 (1989).
5. C. Kittell, *Introduction to Solid State Physics* (Wiley, New York, 1976).
6. L. Stixrude and M. S. T. Bukowinski, *Am Mineral.*, in press.
7. G. O. Brunner and W. M. Meier, *Nature* 337, 146 (1989); W. M. Meier and D. H. Olson, *Atlas of Zeolite Structure Types* (Butterworth Kent, UK, 1988).
8. Liquid-crystal density inversion is important geologically because it determines the direction (up or down) of liquid transport in Earth and thereby the direction of terrestrial chemical evolution. It implies that magmas produced below a certain depth, instead of rising to the surface, will sink to greater depths. Other factors that probably contribute to the density inversion are element partitioning, particularly of Fe [C. B. Agee and D. Walker, *J. Geophys. Res.* 93, 3437 (1988)], and coordination changes in the liquid (*9*). The latter is expected to occur at higher pressures (20 to 30 GPa, corresponding to the upper mantle–lower mantle boundary region near 670 km depth) than the compression mechanisms we described.
9. Q. Williams and R. Jeanloz, *Science* 239, 902 (1988); X. Xue, J. F. Stebbins, M. Kanzaki, R. G. Trønnes, *ibid.* 245, 962 (1989).
10. For each pressure, we initiated one 2000 K simulation by isobarically cooling the equilibrated 6000 K liquid directly to 2000 K and the other by first isobarically cooling the 6000 K liquid to 4000 K and re-equilibrating it at this intermediate temperature before finally isobarically cooling it to 2000 K. The simulations are identical to those in (*4*), which contains a detailed description of the method.
11. C. S. Marians and L. W. Hobbs, *J. Non-Cryst. Solids*, in press. A fundamental ring is defined as one which cannot be divided into two smaller ones. Thus, the new definition explicitly resolves the ambiguities which were often caused, under previous definitions, by the potential division of large rings. Furthermore, while previous definitions consider only six rings per T-atom, the new definition allows for the common occurrence of greater ring populations (*6*) (cristobalite, for example, contains 12 six-membered rings per T-atom). See (*6*) and J. V. Smith [*Am. Mineral.* 62, 703 (1977)] for critical discussions of the definition of a ring.
12. The four-coordinate Bethe lattice is the simplest possible tetrahedral framework because it contains no rings. It consists of a central atom, its four first-linked neighbors, the three additional atoms linked to each of these four for a total of $4 \times 3 = 12$ second-linked neighbors, $12 \times 3 = 36$ third-linked neighbors, and so on. The inset of Fig. 2 illustrates a four-coordinate Bethe lattice complete through the third-linked neighbor shell.
13. The number of Q^{th}-linked neighbors in the four-coordinate Bethe lattice is $4 \times 3^{Q-1}$. One can show, then, that the total number of atoms pruned from a Bethe lattice complete through the Q^{th}-linked neighbor shell, $P(Q,K)$, by the formation of a ring of size K is $3^{Q-S} - 1$ for odd K, and $2 \times 3^{Q-S} - 1$ for even K, where S is the linked neighbor shell in which a ring closes: S is $(K - 1)/2$ for odd rings, and $K/2$ for even rings (*6*). The expression (Eq. 1) for the relative pruning efficiency, $P^*(K)$, is derived by taking the large Q limit of $P(Q,K)$ normalized to $P(Q,3)$

$$P^*(K) = \lim_{Q \to \infty} P(Q,K)/P(Q,3)$$

14. We thank R. Jeanloz, H. Zhang, and two anonymous referees for helpful comments on the manuscript. This work was supported by National Science Foundation grant EAR-8816819 and the Institute of Geophysics and Planetary Physics at the Lawrence Livermore Laboratory. The latter along with the San Diego Supercomputer Center and the University of California, Berkeley, Computing Center, provided generous supercomputer support.

14 May 1990; accepted 6 August 1990

Tetraplex Formation of a Guanine-Containing Nonameric DNA Fragment

RENZHE JIN, KENNETH J. BRESLAUER, ROGER A. JONES, BARBARA L. GAFFNEY*

A combination of spectroscopic and calorimetric techniques has been used to characterize the structures formed by a family of short, guanine-containing DNA single strands of the form d[GGTTXTTGG], X = A, C, G, T. In 1 molar NaCl at low temperatures, these molecules do not behave like single strands, but rather exhibit properties consistent with tetraplex formation. The standard state enthalpies, entropies, and free energies for formation of each tetraplex have been measured, as have preliminary nuclear magnetic resonance (NMR) spectra. In 1 molar KCl, the melting behavior of the structure or structures is more complex than in 1 molar NaCl. This observation may be related to the recently proposed "sodium-potassium switch."

A FOUR-STRANDED FORM OF DNA with guanine self-pairing (so-called G4 DNA) has been proposed by Sen and Gilbert (*1*) to play a key role in meiosis. In this tetraplex model, repetitive, guanine-rich regions initiate the required alignment of four chromatids by formation of parallel, four-stranded structures in which sets of four guanine bases are arranged in planar tetrads by means of Hoogsteen hydrogen bonding (Fig. 1). Guanine-rich regions occur both at the ends of chromosomes, called telomeres (*2*), and within them, at recombination hot spots (*3*). Guanine tracts also occur in gene regulatory regions (*4*). For these reasons, guanine tetrads may represent biologically significant structures that participate in functionally important mechanisms. Several closely related models involving guanine self-pairing have been proposed recently for the specialized structures that occur in telomeres. The guanine-rich strand at the end of many chromosomes is 12 to 16 bp longer than the cytosine-rich strand and may fold back on

Department of Chemistry, Rutgers, The State University of New Jersey, Piscataway, NJ 08855.

*To whom correspondence should be addressed.

Table 1. Thermodynamic data for complex formation by [GGTfs4uTXTTGG].

Strand	T_{max}* (°C)	$\Delta H°_{cal}$† (kcal/mol)	n	$4{\cdot}\Delta H°_{cal}$ (kcal/mol)	$\Delta H°_{vH}$‡ (kcal/mol)	$\Delta S°_{vH}$‡ (cal/mol·deg)	$\Delta G°$§ (kcal/mol)
X = T	22.6	−27.6	3.9	−110	−112	−325	−15
X = G	21.3	−23.6	3.7	−94	−97	−276	−14
X = A	19.3	−26.9	3.7	−108	−110	−323	−14
X = C	15.5	−25.0	3.7	−100	−103	−304	−12

*Total concentration of strands = 10^{-4} M. †Average of three DSC scans. ‡Calculated with n = 4. §Calculated at 25°C.

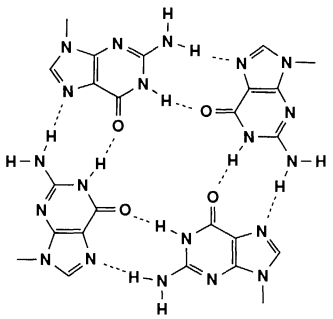

Fig. 1. Putative structure of the guanine tetrad.

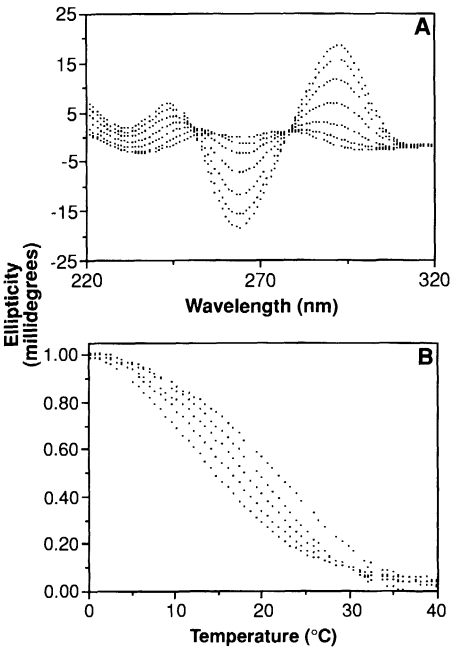

Fig. 2. (**A**) Temperature-dependent CD spectra for d[GGTTTTTGG] in 10 mM phosphate, 0.1 mM EDTA, 1.0 M sodium, pH 7. Identifying the spectra from top to bottom at 290 nm, temperatures are 0°, 5°, 10°, 15°, 20°, 25°, and 50°C. Samples were pre-equilibrated at 0°C for 1 hour. Spectra were recorded with a model 60 DS AVIV circular dichroism spectropolarimeter. Each spectrum is the average of three scans from which the buffer background was subtracted. Spectra for the molecules d[GGTTXTTGG], X = A, C, G, are similar. (**B**) CD melting curves recorded at 290 nm for d[GGTTTTTGG] in 10 mM phosphate, 0.1 mM EDTA, 1.0 M sodium, pH 7, at total strand concentrations from left to right of 10, 20, 40, 80, and 120 μM. Ellipticities at 0°C were normalized to 1.00. Samples were heated at a rate of 1°C/min. Curves for the molecules d[GGTTXTTGG], X = A, C, G, in 1 M NaCl are similar.

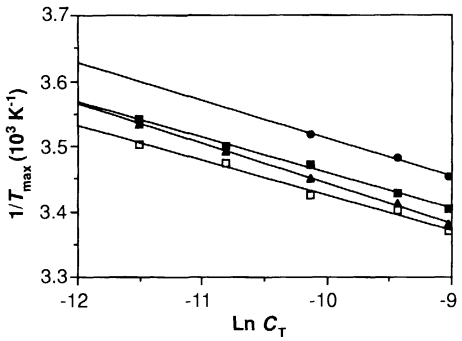

Fig. 3. Plots of $1/T_{max}$ versus ln C_T for the molecules d[GGTTXTTGG], X = A (■), C (●), G (▲), and T (□).

itself (*5*). Unimolecular structures with guanine tetrads formed from intramolecular interactions have been proposed for $d[T_4G_4]_4$ and $d[T_2G_4]_4$ (*6*) and for $d[G]_{27}$ and $d[G]_{37}$ stretches inserted into restriction fragments (*7*). Folded-back hairpins that dimerize to give bimolecular structures have been suggested for the shorter oligomers $d[T_4G_4]_2$ and $d[T_2G_4]_2$ (*6*), as well as for a duplex 29 bp long with a $d[T_2G_4]_2$ overhang (*8*). Thus DNA seems to be versatile enough to utilize the base-pairing properties of guanine in a variety of ways, both inter- and intramolecularly, to form non–Watson-Crick structures that may be functionally important.

Structures involving base tetrads have been proposed for quite some time, both for monomeric guanosine derivatives (*9, 10*) and for the polymers poly rG and polyriboinosine (poly rI) (*11–13*). More recently, a similar structure has been proposed for the dimer d[GpG] (*14*). Several of these early investigators also have proposed that certain monovalent cations specifically chelate in the centers of the base tetrads (or between them), thereby potentially providing a major driving force for tetrad formation (*10*).

Sen and Gilbert recently have extended their original work on four-stranded DNA complexes to include many more examples, all of which appear to form tetraplexes in the presence of sodium ion (*15*). By contrast, in the presence of potassium ion, the molecules with at least two separated runs of guanines appear only to form hairpin dimers similar to those found by others (*6, 8*). To explain this and related observations, Sen and Gilbert proposed a "sodium-potassium switch" that may have biological significance (*15*).

In the study reported here, we present evidence that a family of short DNA single strands with tracts of only two guanines, d[GGTTXTTGG], X = A, C, G, T, forms tetraplexes in 1 M NaCl at low temperatures. The tetramolecular nature of the complex is supported by a thermodynamic analysis of spectroscopic and calorimetric data. We also report $\Delta H°$, $\Delta S°$, and $\Delta G°$ for the formation of each tetraplex from its parent single strand, as well as preliminary NMR characterization of one of them in 1 M NaCl.

The circular dichroism (CD) spectra for each strand, d[GGTTXTTGG], X = A, C, G, T, exhibit a dramatic temperature dependence (Fig. 2A). This dependence contrasts markedly with the CD spectra of the complementary single strands, d[CCAAYAACC], Y = A, C, G, T, which do not change appreciably with temperature and which do not contain guanine tracts. For the d[GGTTXTTGG] strands, the temperature-dependent CD change is largest near 290 nm. Plots of molar ellipticity at 290 nm versus temperature show surprisingly sharp monophasic melting transitions (Fig. 2B). For two of the molecules (X = T and X = G), salt-dependent CD melting studies reveal that the thermally induced transition is not observed at 16 mM NaCl, but is observed at 213 mM NaCl and becomes progressively more pronounced as the salt concentration is increased to 1 M NaCl. These data are consistent with the formation of a complex with a high charge density that is stabilized by a high salt concentration. In contrast with the melting behavior in 1 M NaCl, the melting profile of a sample of d[GGTTTTTGG] in 1 M KCl, pre-equilibrated at 25°C for 48 hours, is multiphasic. This result may be consistent with the "sodium-potassium switch" proposed by Sen and Gilbert (*15*).

The corresponding ultraviolet (UV) absorption melting profiles exhibit a significant but much less dramatic hypochromicity (10%) for thermal disruption of the complex, which is consistent with our previous observations of these molecules (*16*). Thus in this system CD is a more sensitive technique than UV absorption for monitoring these thermally induced transitions.

For each complex, we used the concentration dependence of the CD melting temperatures in conjunction with the corresponding calorimetrically measured transition enthalpy ($\Delta H°$) to calculate the number of single strands n that self-associate to form each complex (the so-called molecularity n). We also used the spectroscopic and calorimetric data to characterize thermodynami-

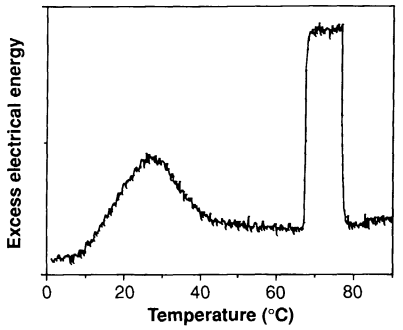

Fig. 4. Excess electrical energy versus temperature for d[GGTTTTTGG] in 10 mM phosphate, 0.1 mM EDTA, 1.0 M sodium, pH 7, recorded with a Microcal MC-2 differential scanning calorimeter. Note that the calorimetric transition is accompanied by an apparent small and positive heat capacity change that may reflect differential solvent accessibility to the four strands in the initial and final states. Samples were pre-equilibrated for 2 hours at −2°C and then heated at a rate of 1°C/min. The square-wave function near 70°C corresponds to an electrical calibration, the area under which is equal to 8.512 mcal. The total strand concentration is 0.28 mM. Profiles for the molecules d[GGTTXTTGG], X = A, C, G, are similar.

cally the stability ($\Delta G°$) and the melting behavior ($\Delta H°$ and $\Delta S°$) of each complex.

It is possible to calculate the van't Hoff enthalpy ($\Delta H°_{vH}$), entropy ($\Delta S°_{vH}$), and free energy ($\Delta G°$) for a two-state transition by measuring how the temperature midpoint (T_m) of the CD melting curves (or the temperature maximum or minimum, T_{max}, of the differentiated CD melting curves) varies with strand concentration, C_T, (*17*). The relevant general equations, in which R is the gas constant, are:

$$\frac{1}{T_m} = \frac{R(n-1)}{\Delta H°_{vH}} \ln C_T + \frac{\Delta S°_{vH} - (n-1)R\ln 2 + R\ln n}{\Delta H°_{vH}} \quad (1a)$$

$$\frac{1}{T_{max}} = \frac{R(n-1)}{\Delta H°_{vH}} \ln C_T + \frac{\Delta S°_{vH}}{\Delta H°_{vH}} + \frac{R\{[(2+n)/2]\ln n - (n-1)\ln (n^{1/2}+1)\}}{\Delta H°_{vH}} \quad (1b)$$

Note that these equations imply a linear relation between $1/T_m$ (or $1/T_{max}$) and ln C_T, since each equation has the form $y = mx + b$. Thus, from the molecularity n one can calculate $\Delta H°_{vH}$, $\Delta S°_{vH}$, and $\Delta G°$ from the slope and intercept of a $1/T_m$ (or $1/T_{max}$) versus ln C_T plot, such as is shown in Fig. 3 (*17*). However, if one has an independent measure of the transition enthalpy, Eqs. 1a or 1b can be used in a less traditional manner to calculate n, the molecularity of a complex. Differential scanning calorimetry (DSC) provides such an independent measure of $\Delta H°$. We have used DSC to determine the transition enthalpy per strand, $\Delta H°_{cal}$, for each complex from the area under the corresponding experimental heat capacity versus temperature curve (Fig. 4) and knowledge of the total strand concentration. Repeated DSC scans produced superimposable melting profiles, thereby demonstrating the reversibility of the transition. If the transition can be approximated by an all-or-none transformation, and if ΔC_p is negligible over the temperature range studied, then $n\Delta H°_{cal}$ approximately will be equal to the van't Hoff enthalpy, $\Delta H°_{vH}$ (*17*). Thus the calorimetrically measured value $n\Delta H°_{cal}$ can be used to define $\Delta H°_{vH}$ in Eqs. 1a or 1b. For each complex, the slope of the $1/T_m$ (or $1/T_{max}$) versus ln C_T plot (Fig. 3) is equal to $[R(n-1)/n\Delta H°_{cal}]$, the ln C_T coefficient in Eqs. 1a and 1b. Thus, on the basis of this relation, we can write a general expression for the molecularity n, which in fact represents the average molecularity of all species present in solution.

$$n = \frac{R}{R - [(\text{slope})\Delta H°_{cal}]} \quad (2)$$

We have calculated the values of n listed in Table 1 using the above approach. In principle, these molecules, which contain two separated guanine tracts, could form tetrad structures such as hairpin dimers, for which n would equal 2, or tetraplexes, for which n would equal 4. Note that for all of the complexes studied here, n approximately is equal to 4. Thus, in the absence of fortuitous compensation due to a mixture of species and/or the approach of polymer behavior (*17*), the thermodynamic evidence is consistent with the formation of tetraplexes rather than hairpin dimers under the conditions of this study (*18*).

Given this determination of average molecularity, the thermodynamic parameters $\Delta H°_{vH}$, $\Delta S°_{vH}$, and $\Delta G°$ for the transition from single strands to associated tetraplex can then be calculated from Eqs. 1a or 1b using $n = 4$. Specifically, ΔH_{vH} can be calculated from the slope, $\Delta S°_{vH}$ can be calculated from the y intercept, and $\Delta G°$ can be calculated at 25°C from $\Delta G° = \Delta H° - T\Delta S°$ (Table 1). Inspection of the $\Delta G°$ data reveals that these nonameric tetraplexes exhibit considerable stability. On a per strand basis, the tetraplex stabilities at 25°C ($\Delta G°$) are similar in magnitude to those of the corresponding Watson-Crick duplexes (*16*). A detailed comparison of the thermodynamic data based on molecular interactions within the duplex and tetraplex structures is not yet possible because of the unknown nature of the specific interactions that occur within the tetraplex structure.

One-dimensional ^{1}H NMR spectra were recorded both in H_2O and D_2O. The nonexchangeable sugar H_1 protons appear in the D_2O spectrum, at 0°C, between 5.6 and 6.8 ppm as five singlets and one multiplet that integrates for four protons relative to each singlet (Fig. 5A). The fact that more peaks are not present is consistent with, but does not prove, the presence of predominantly one species.

The H_2O spectrum at −1°C exhibits three sharp resonances in the ratio of 1:1:2 between 11.7 and 12.3 ppm and three very broad resonances between 9.5 and 11.0 ppm (Fig. 5B). Upon heating to 15°C, the three sharp peaks resolve into four without visible broadening. However, the very broad peaks almost disappear by 15°C. At 30°C, the sharp peaks are still present, although diminished in intensity, and disappear by 50°C. The four sharp peaks may correspond to the four guanine H1 protons, which would be expected to exchange much more slowly in these structures than the

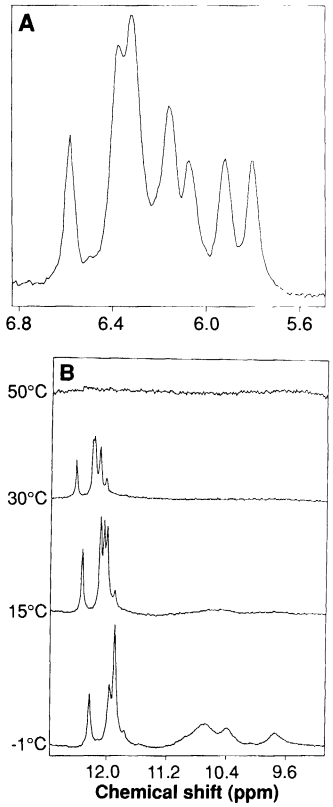

Fig. 5. Proton NMR spectrum (**A**) for d[GGTTTTTGG] at 0°C in 10 mM phosphate, 0.1 mM EDTA, 1.0 M sodium, pH 7, in D_2O, and (**B**) for d[GGTTTTTGG] at the indicated temperatures in 10 mM phosphate, 0.1 mM EDTA, 1.0 M sodium, pH 7, in 90% H_2O/10% D_2O, where the chemical shift scale is for the −1°C spectrum only. The total strand concentration is 1.8 mM. Spectra were recorded on a XL-400 Varian 400-MHz NMR spectrometer.

thymine H3 protons.

Guanine-containing DNA fragments recently have been shown to form unusual structures that seem to utilize guanine tetrads to stabilize unimolecular (*6, 7*), bimolecular (*6, 8*), and tetramolecular (*1, 15*) associations. In this report we have described a new example of a tetramolecular complex, one comprised of strands only 9 bp long and therefore suitable for detailed characterization. Biological processes may take advantage of all of these guanine-tetrad–containing structures. For example, four duplexes may form tetraplexes while initiating alignment during meiosis (*1, 15*). Guanine-rich regions within two chromatids may form hairpins and then dimerize, thereby aligning and pairing the strands for recombination (*8*). Dimerization also may occur at telomeric ends (*6, 8*). The guanine-rich strand of a single duplex may separate from its complementary strand to form its own structure, either within the strand (*7*), possibly as part of H DNA (*19*), or at its end (*6*). Control of these different forms may depend in part on a "sodium-potassium switch" (*15*). Furthermore, these guanine self-paired structures may interact with proteins. For example, the enzyme human DNA(cytosine-5)methyltransferase recently was proposed to act at a possible G4-DNA/B-DNA junction at codon 12 of c-H-*ras* (*20*). In addition, the enzyme called telomere terminal transferase appears specifically to act on specialized telomere structures (*21*). Guanine self-associations also may influence RNA structure since guanine tetrads have been postulated to form between strands of poly rG (*11*). Additional biophysical studies on specially designed and synthesized DNA and RNA fragments should help to elucidate the potential role that these guanine associations play in biological systems.

REFERENCES AND NOTES

1. D. Sen and W. Gilbert, *Nature* **334**, 364 (1988).
2. E. H. Blackburn and J. W. Szostak, *Annu. Rev. Biochem.* **53**, 163 (1984).
3. T. Nikaido, Y. Yamawaki-Kataoka, T. Honjo, *J. Biol. Chem.* **257**, 7322 (1982); A. J. Jeffreys, V. Wilson, S. L. Thein, *Nature* **314**, 67 (1985); D. A. Collier, J. A. Griffin, R. D. Wells, *J. Biol. Chem.* **263**, 7397 (1988); N. D. Hastie and R. C. Allshire, *Trends Genet.* **5**, 326 (1989).
4. J. M. Nickol and G. Felsenfeld, *Cell* **35**, 467 (1983); T. Evans, E. Schon, G. Gora-Maslak, J. Patterson, A. Efstratiadis, *Nucleic Acids Res.* **12**, 8043 (1984); M. W. Kilpatrick, A. Torri, D. S. Kang, J. A. Engler, R. D. Wells, *J. Biol. Chem* **261**, 11350 (1986); C. J. Pears and J. G. Williams, *Nucleic Acids Res.* **16**, 8467 (1988).
5. E. Henderson, C. C. Hardin, S. K. Walk, I. Tinoco, Jr., E. H. Blackburn, *Cell* **51**, 899 (1987); E. R. Henderson and E. H. Blackburn, *Mol. Cell. Biol.* **9**, 345 (1989).
6. J. R. Williamson, M. K. Raghuraman, T. R. Cech, *Cell* **59**, 871 (1989).
7. I. G. Panyutin *et al.*, *Proc. Natl. Acad. Sci U S.A.* **87**, 867 (1990).
8. W. I. Sundquist and A. Klug, *Nature* **342**, 825 (1989).
9. M. Gellert, M. N. Lipsett, D. R. Davies, *Proc. Natl. Acad Sci. U.S.A.* **48**, 2013 (1962); J. F. Chantot, M. Sarocchi, W. Guschlbauer, *Biochimie* **53**, 347 (1971); S. B. Zimmerman, *J. Mol. Biol* **106**, 663 (1976).
10. T. J. Pinnavaia *et al.*, *J Am. Chem Soc.* **100**, 3625 (1978); M. Borzo, C. Detellier, P. Laszlo, A. Paris, *ibid.* **102**, 1124 (1980).
11. S. B. Zimmerman, G. H. Cohen, D. R. Davies, *J. Mol. Biol.* **92**, 181 (1975).
12. S. Arnott, R. Chandrasekaran, C. M. Marttila, *Biochem. J.* **141**, 537 (1974).
13. F. B. Howard and H. T. Miles, *Biochemistry* **21**, 6736 (1982).
14. P. Mariani, C. Mazabard, A. Garbesi, G. P. Spada, *J. Am. Chem. Soc.* **111**, 6369 (1989).
15. D. Sen and W. Gilbert, *Nature* **344**, 410 (1990).
16. B. L. Gaffney and R. A. Jones, *Biochemistry* **28**, 5881 (1989).
17. K. J. Breslauer, in *Thermodynamic Data for Biochemistry and Biotechnology*, H. J. Hinz, Ed. (Springer-Verlag, New York, 1986), pp. 402–427; L. A. Marky and K. J. Breslauer, *Biopolymers* **26**, 1601 (1987).
18. Preliminary ultracentrifugation measurements in 1 M NaCl, conducted in collaboration with E. Braswell, suggest that more than one species may be present under the centrifugation conditions. However, meaningful interpretation of these data demands an understanding of the relative contributions of any competing equilibria, which in turn requires careful modeling and fitting.
19. V. I. Lyamichev *et al.*, *Nature* **339**, 634 (1989).
20. S. S. Smith, D. J. Baker, L. A. Jardines, *Biochem Biophys. Res. Commun.* **160**, 1397 (1989).
21. D. Shippen-Lentz and E. H. Blackburn, *Mol. Cell. Biol* **9**, 2761 (1989); C. W. Greider and E. H. Blackburn, *Cell* **51**, 887 (1987).

22. Supported by grants from the National Institutes of Health GM31483 (R.A.J.), GM23509 (K.J.B.) and an American Cancer Society Faculty Research Award to R.A.J.

30 May 1990; accepted 21 August 1990

Underexpression of β Cell High K_m Glucose Transporters in Noninsulin-Dependent Diabetes

JOHN H. JOHNSON, ATSUSHI OGAWA, LING CHEN, LELIO ORCI, CHRISTOPHER B. NEWGARD, TAUSIF ALAM, ROGER H. UNGER*

The role of defective glucose transport in the pathogenesis of noninsulin-dependent diabetes (NIDDM) was examined in Zucker diabetic fatty rats, a model of NIDDM. As in human NIDDM, insulin secretion was unresponsive to 20 mM glucose. Uptake of 3-*O*-methylglucose by islet cells was less than 19% of controls. The β cell glucose transporter (GLUT-2) immunoreactivity and amount of GLUT-2 messenger RNA were profoundly reduced. Whenever fewer than 60% of β cells were GLUT-2–positive, the response to glucose was absent and hyperglycemia exceeded 11 mM plasma glucose. We conclude that in NIDDM underexpression of GLUT-2 messenger RNA lowers high K_m glucose transport in β cells, and thereby impairs glucose-stimulated insulin secretion and prevents correction of hyperglycemia.

TYPE 2 OR NONINSULIN-DEPENDENT diabetes (NIDDM), the most common hyperglycemic syndrome of man, is ascribed to a declining capacity of pancreatic β cells to compensate for underlying insulin resistance by increased secretion of insulin (*1*). The mechanism of this genetically determined β cell decompensation is obscure; β cells of NIDDM patients appear morphologically normal (*2*). The loss of acute insulin response to glucose in such patients is not accompanied by a parallel impairment in the insulin response to non-glucose secretagogues (*3*). This observation points to a glucose-specific defect in the pathway for insulin secretion. Transmembrane glucose transport is one possible site of such a defect (*4–6*).

Here we report that in a rodent model of NIDDM, hyperglycemia in excess of 11 mM is invariably associated with selective β cell unresponsiveness to glucose, reduced glucose transport in islets, and high K_m (Michaelis constant) underexpression of the high K_m glucose transporter of β cells (GLUT-2). We propose that these abnormalities are causally linked.

We employed as a model of NIDDM a colony of partially inbred Zucker diabetic fatty (ZDF) rats [ZDF/Drt-*fa*(F10)] (*7*). In this colony, all of the males develop obesity, insulin resistance, and overt NIDDM between the seventh and ninth week of life. By 10 weeks of age, their average plasma glucose level exceeds 22 mM. The female littermates also develop obesity and insulin resistance but do not become overtly diabetic, presumably because their β cells maintain sufficient glucose-responsive insulin secretion to compensate for the resistance.

To determine whether, as in human NIDDM, β cells of overtly diabetic ZDF rats are insensitive to glucose, we studied

Center for Diabetes Research, University of Texas, Southwestern Medical Center, 5323 Harry Hines Boulevard, Dallas, TX 75235.

*To whom correspondence should be addressed.